Journal of Power Sources 219 (2012) 333–338

Contents lists available at SciVerse ScienceDirect

Journal of Power Sources

journal homepage: www.elsevier.com/locate/jpowsour

Improved cycling performance of 5 V spinel $LiMn_{1.5}Ni_{0.5}O_4$ by amorphous $FePO_4$ coating

Dilong Liu, Ying Bai*, Sen Zhao, Weifeng Zhang*

Key Laboratory of Photovoltaic Materials of Henan Province and School of Physics & Electronics, Henan University, Jinming Street 1, Kaifeng 475004, PR China

HIGHLIGHTS

► $FePO_4$ coating layer enhances the cycling stability of $LiMn_{1.5}Ni_{0.5}O_4$.
► The optimum coating content of $FePO_4$ was found to be 1 wt.%.
► $FePO_4$ separation can effectively suppress the formation of thick SEI layer.
► $FePO_4$ modification enhances surface kinetics of $LiMn_{1.5}Ni_{0.5}O_4$ material.

ARTICLE INFO

Article history:
Received 25 March 2012
Received in revised form
5 June 2012
Accepted 21 July 2012
Available online 27 July 2012

Keywords:
Spinel $LiMn_{1.5}Ni_{0.5}O_4$
Iron phosphate ($FePO_4$)
Cycling performance
Surface coating
Lithium-ion batteries (LIBs)

ABSTRACT

Cycling stability of 5 V spinel $LiMn_{1.5}Ni_{0.5}O_4$ (LMNO) is improved by surface modification with $FePO_4$ through a chemical deposition method. The pristine, 0.5 wt.%, 1 wt.% and 3 wt.% $FePO_4$-coated LMNO are characterized by X-ray diffraction, Fourier transform infrared spectroscopy, transmission electron microscopy and field emission scanning electron microscopy. It is found that the coating process is in favor of the disorder–order phase transition. The investigation on their cycling performance demonstrates that 1 wt.% $FePO_4$-modified LMNO cathode exhibits the best cycling performance, with the capacity retention ratio of 99.3% after 50 cycles, much better than that of the pristine LMNO (only 79%). Electrochemical impedance spectroscopy is applied to explain the galvanostatic results. The enhanced cycling performance of the surface-modified samples can be attributed to the decreasing contact area between the electrode and electrolyte and the suppression of undesirable thick SEI (solid electrolyte interfacial) layer.

1. Introduction

Lithium-ion batteries (LIBs), for their high gravimetric and volumetric energy densities, are being urgently pursued for electric vehicle (EV), hybrid electric vehicle (HEV) and plug-in hybrid electric vehicle (PHEV) applications to alleviate the environmental and energy pressures [1]. To obtain more recyclable energy, various active materials for potential cathodes have been proposed in the past two decades. Considering the intrinsic excellent rate performance arising from the three-dimensional path of lithium ions in the spinel lattice, as a derivative of spinel $LiMn_2O_4$, the spinel $LiMn_{1.5}Ni_{0.5}O_4$ (LMNO) has recently attracted great attentions [2–11] for its nearly flat operating voltage [12,13]. It shows a high capacity of 130 mAh g^{-1} (theoretical capacity: 147 mAh g^{-1}) and much higher operating voltage at around 4.7 V, which is attributed to the Ni^{2+}/Ni^{3+} and Ni^{3+}/Ni^{4+} redox couples [3,5].

However, this material has non-negligible drawbacks such as the formation of $Li_xNi_{1-x}O$ impurity phase during the synthesis process [4,8,14–16], cathode surface and electrolyte instability at high operating voltage above 4.8 V [17]. To solve the former problem, various synthesis routes and partial substitution by other cations pursued in recent studies have successfully suppressed the formation of $Li_xNi_{1-x}O$ impurity phase and stabilized the spinel structure. Since the formation of thick solid electrolyte interface (SEI) film at high operating voltage has been confirmed one of the major factors leading to capacity fading, surface modification by various inactive materials, such as ZnO, Al_2O_3, $AlPO_4$, Bi_2O_3 and carbon [12,18–21] have also been proved to be an effective method to solve the latter problem and improve the electrochemical performances of LMNO cathode. Among the surface modification studies, it has been found that the improved electrochemical behavior can be attributed to the suppression of the growth of SEI film and the partial suppression of stress caused by the volume change during cycling [20].

$FePO_4$ has been advanced to be a novel cathode candidate for LIBs because of its various advantages such as environmental friendliness, low cost and thermal stability [22,23]. As

* Corresponding authors. Tel.: +86 378 3880 696; fax: +86 378 3880 659.
E-mail addresses: ybai@henu.edu.cn (Y. Bai), wfzhang@henu.edu.cn (W. Zhang).

0378-7753/$ – see front matter © 2012 Elsevier B.V. All rights reserved.
http://dx.doi.org/10.1016/j.jpowsour.2012.07.058

a modification material, $FePO_4$ has been coated on the surface of $LiCoO_2$ [22], $Li_xNi_{0.9}Co_{0.1}O_2$ [24] and $LiMn_2O_4$ [25]. Similarly, these studies show significantly improved electrochemical performances after modification. Clearly, $FePO_4$ is chemically-stable and electrochemically-active, which is desirable to be a coating material. In this paper, the effects of $FePO_4$ coating on the electrochemical performances of LMNO are investigated and reported for the first time. Experimental results show that 1 wt.% $FePO_4$-coated LMNO electrode exhibits excellent cycling stability compared with its pristine counterpart.

2. Experimental

Pristine LMNO was synthesized by sol–gel method as described in Ref. [26]. Stoichiometric amounts of $CH_3COOLi\cdot 4H_2O$ (Aldrich), $Mn(CH_3COO)_2\cdot 4H_2O$ (Aldrich), $Ni(CH_3COO)_2\cdot 4H_2O$ (Aldrich) and citric acid (Aldrich) were dissolved in distilled water uniformly, wherein the mole ratio between total transition metal ions and citric acid was fixed at 1:1.5 [23]. With vigorous stirring, ammonium hydroxide was slowly added into the mixture to keep the pH value about 7.0 constantly. Subsequently, the mixture was stirred intensely at 80 °C till viscous gel was formed, then the gel was preheated at 350 °C for 6 h to combust the organic components. After the residual powder was ground, it was eventually heated at 800 °C for 10 h with a heating and cooling rate of 5 °C min^{-1}. LMNO was obtained and used as the pristine material for the following study.

To prepare $FePO_4$-coated (0.5, 1 and 3 wt.%) LMNO samples, $Fe(NO)_3\cdot 9H_2O$ (Aldrich) and pristine LMNO were dispersed and mixed in distilled water with vigorous stirring. Afterwards, $(NH_4)_2HPO_4$ solution was added drop by drop into the mixture. The actual usage of $Fe(NO_3)_3$ are 6.7 mg, 13.4 mg and 40.8 mg, and the usage of $(NH_4)_2HPO_4$ are 2.3 mg, 4.5 mg and 13.4 mg for the preparation of 0.5 wt.%, 1 wt.% and 3 wt.% $FePO_4$-coated LMNO samples respectively. Naturally, $FePO_4$ was formed and deposited onto the surface of LMNO particles. After repeated rinsing and filtering, the filtered precipitation was heated at 550 °C for 6 h. Finally, the $FePO_4$-coated LMNO samples were obtained.

X-ray diffraction (XRD) patterns of the samples were collected by a Philips PANA-lytical X' pert X-ray diffractometer equipped with a monochromatized Cu $K\alpha_1$ radiation between 10° and 80° at a scan rate of 0.02° s^{-1}. Fourier transform infrared (FTIR) spectroscopy was applied to examine the ordering of cations in 16d sites of the spinel lattice and were recorded with KBr pellet by an AVATAR360 Fourier-transformed infrared spectrometer. The surface morphology of samples was observed through field emission scanning electron microscopy (FESEM, JEOL JSM-6390LV). Electron diffraction spectroscopy (EDS) was applied to determine the elements of powders together with SEM in large field of view. The inductively coupled plasma (ICP) analysis was performed on Shimazu ICP-8000. The images of high resolution transmission electron microscopy (HRTEM) was collected on JEOL JEM 2010 equipment to investigate the microstructure of samples.

Electrode sheets were prepared with mixing 80 wt.% active material, 10 wt.% carbon black and 10 wt.% PVDF (Polyvinylidene Fluoride) to form a homogeneous slurry. Afterwards, the electrode sheets were dried at 120 °C for 12 h under vacuum, and cut into squares with area of 0.64 cm^2. Lithium metal and Celgard 2300 were used as counter electrode and separator, respectively. 1 M $LiPF_6$ dissolving in EC/DEC (1:1 volume ratio of ethylene carbonate/diethyl carbonate) was used as electrolyte. Batteries were fabricated in an argon filled glove-box with H_2O and O_2 contents less than 1 ppm. Cycling performances were evaluated with a Neware battery tester (CT-3008W-5V3A-S4) between 4.9 and 3.5 V. EIS (electrochemical impedance spectroscopy) investigations were performed using an electrochemical workstation with three electrode systems (CHI660C, Shanghai). Experiments were carried out after the cells were charged and discharged completely at different cycles followed by potentiostatically holding at 3.5 V for 48 h with an AC amplitude of 10 mV in the frequency range of 10^5 Hz to 5 m Hz using the former electrochemical workstation.

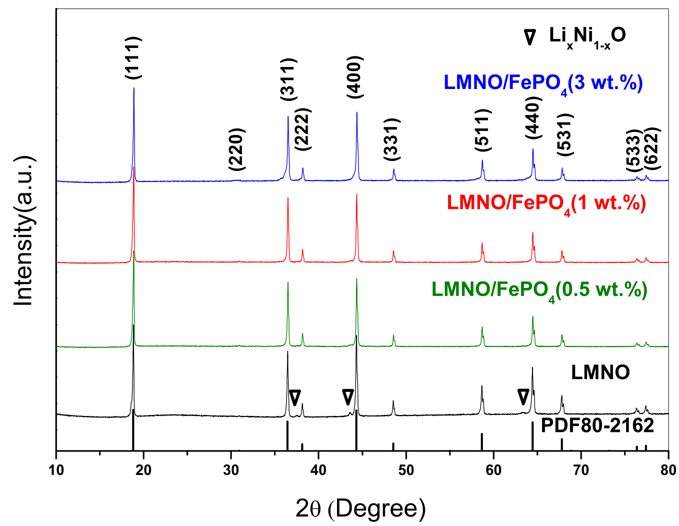

Fig. 1. XRD patterns of pristine and surface-modified LMNO samples.

3. Results and discussion

It is known that under certain circumstances the series of high-voltage spinels LMNO can exhibit 3/1 transition metal ordering on the 4b and 12d octahedral sites of space group $P4_332$ versus random octahedral 16 sites of Fd3m [27]. The LMNO spinel structure can be ordered ($P4_332$) or disordered (Fd3m) framework. The XRD patterns of pristine and modified samples are shown in Fig. 1, which confirms the existence of cubic spinel structure. All the diffraction peaks agree well with those in PDF card 80-2162, assigning to Fd3m space group of the disordered framework. All the main diffraction peaks are sharp, indicating that all the samples are well-crystallized. Minor amount of $Li_xNi_{1-x}O$ can be observed in pristine material due to the deficiency of oxygen since the annealing temperature is higher than the onset temperature located at 712 °C [27]. In comparison, the impurity phase of $Li_xNi_{1-x}O$ disappears in the modified samples. This case can be ascribed to the influence from post-annealing procedure at 550 °C for 6 h. Detailed analysis and discussion will be followed in the FTIR results latter. For its low content or/and intrinsic amorphous structure, no diffraction peak from $FePO_4$ was observed in Fig. 1.

Detailed information can be drawn from the XRD patterns, as shown in Table 1. H. Duncan et al. pointed out that the full width at half maximum (FWHM) of the (400) reflection can be chosen as an indication of the crystallite size [26]. As indicated in Table 1, the lattice parameters and FWHM values are very close for different

Table 1
Lattice parameter, FWHM and intensity ratio obtained from the XRD patterns.

Sample	Lattice parameter (Å)	FWHM (400)	Intensity ratio ($I_{(311)}/I_{(400)}$)
Pristine LMNO	8.2293	0.132	0.7371
0.5 wt.%-coated LMNO	8.2261	0.130	0.8060
1 wt.%-coated LMNO	8.2229	0.128	0.8848
3 wt.%-coated LMNO	8.2163	0.140	0.8845

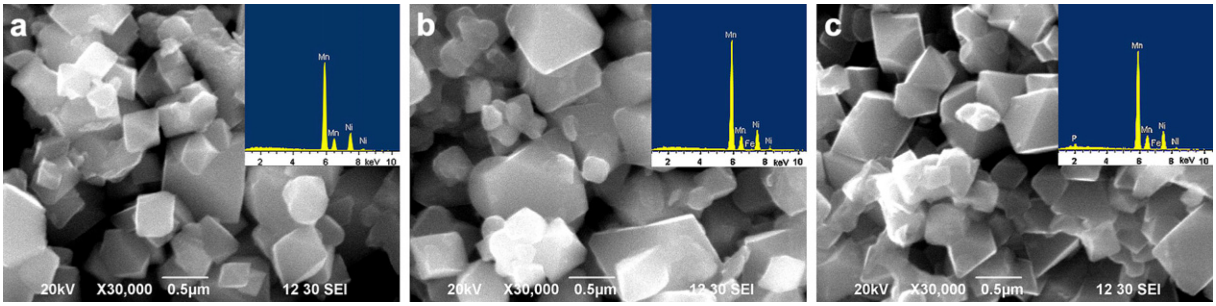

Fig. 2. SEM images and EDS spectra of pristine (a), 1 wt.%-coated (b) and 3 wt.%-coated LMNO (c).

samples, demonstrating the main spinel structure has not been changed after $FePO_4$ surface coating. T.F. Yi et al. reported that the intensity ratio of (311) to (400) peaks was related to the stability of the cubic structure [28]. The $I_{(311)}/I_{(400)}$ values for 0.5, 1 and 3 wt.%-coated LMNO (0.8060, 0.8848 and 0.8845 respectively) are obviously higher than that of the pristine material (0.7371), indicating that $FePO_4$-coated samples have more stable cubic structures compared with the pristine one.

The FESEM measurements were performed to observe the morphologies of the pristine and surface-modified samples. As shown in Fig. 2(a), the pristine LMNO particles are distributed with particle size from 300 to 600 nm, with clean surface and clear boundaries. After surface modification with different contents of $FePO_4$, no obvious difference can be observed from the SEM images, and the particle surface still looks smooth and clean for 0.5 (not shown herein for its morphology looks the same as that of the pristine one), 1 and 3 wt.% $FePO_4$-coated samples (Fig. 2(b) and (c)). The coating layer should be homogeneous and very thin on the LMNO cores, which can be further confirmed directly by HRTEM latter. All the particles in Fig. 2 demonstrate the characteristic shape of spinel phase.

EDS measurement was also performed, and the images are shown in the inset of Fig. 2. No Fe element was detected for LMNO in the inset of Fig. 2(a). Not surprisingly, Fe element was observed for $FePO_4$-coated LMNO (the inset of Fig. 2(b) and (c)). No P element was detected in the inset of Fig. 2(b), maybe due to its low content. ICP analysis shows that the actual contents of $FePO_4$ are 0.43, 1.22 and 2.42 wt.% for the 0.5, 1 and 3 wt.% $FePO_4$-coated LMNO respectively. Nevertheless, we still call 0.5, 1 and 3 wt.% $FePO_4$-coated LMNO in the following discussion.

TEM measurement was applied to observe the microstructure near the particle surface of $FePO_4$-coated samples. Fig. 3 shows the TEM images of the pristine and 1 wt.% $FePO_4$-coated LMNO particles. The pristine LMNO material (Fig. 3(a)) shows good crystallinity with lattice fringe extending to the grain boundary. The crystal orientation of LMNO can be clearly viewed along [111], corresponding to the XRD results. The 1 wt.% $FePO_4$-coated LMNO material (Fig. 3(b)) exhibits an amorphous and uniform modification layer with thickness about 4 nm on the surface. This modification layer of $FePO_4$ will separate the direct contact between the electrode and electrolyte and suppress the side reaction.

Fig. 4 compares the cycling performances of pristine, 0.5, 1 and 3 wt.% $FePO_4$-coated LMNO electrodes with current density of 29.4 mA g^{-1} (C/5 rate) at room temperature. For pristine LMNO, the discharge capacity suffers obvious fluctuation and fast fading (decreased about 27 mAh g^{-1} after 50 cycles, with capacity retention ratio about 79%), though it exhibits a higher initial discharge capacity, about 127 mAh g^{-1}. The formation of unstable SEI (solid electrolyte interphase) layer, as a result of the oxidation of the electrolyte, was considered to be the reason for capacity fading of the pristine LMNO [29]. The initial discharge capacities of 0.5, 1 and 3 wt.% $FePO_4$-coated LMNO electrodes are 126, 121 and 91 mAh g^{-1}, respectively, lower than those of the pristine one. However, the $FePO_4$-coated LMNO electrodes show higher capacity retention ratios in Fig. 4 (87.3%, 99.3% and 103% for 0.5, 1 and 3 wt.% $FePO_4$-coated LMNO electrodes, respectively, after 50 cycles). In this case, an appropriate amount of $FePO_4$ coating is positive in improving the cycling performance, and excessive amount (herein 3 wt.%) acutely decreases the initial capacity of LMNO for the insulating and inactive nature of $FePO_4$.

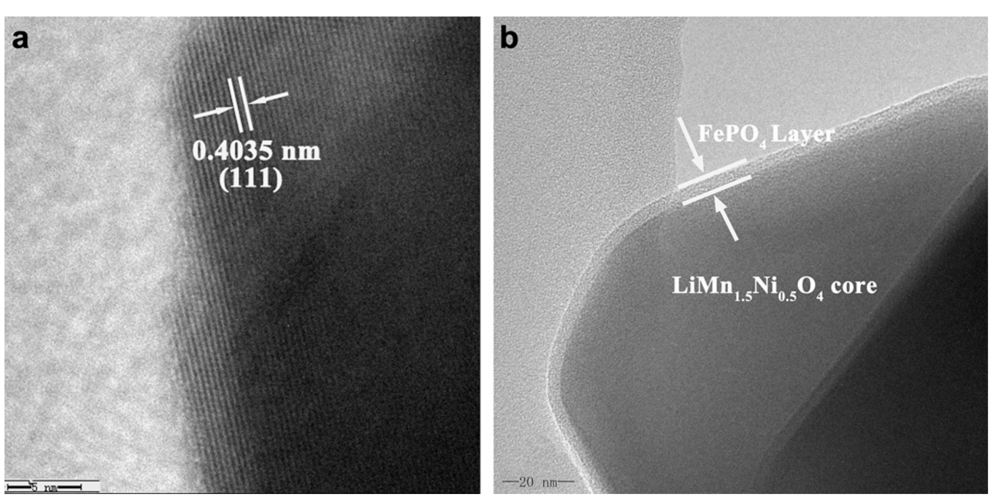

Fig. 3. TEM images of the pristine (a) and 1 wt.% $FePO_4$-coated LMNO (b).

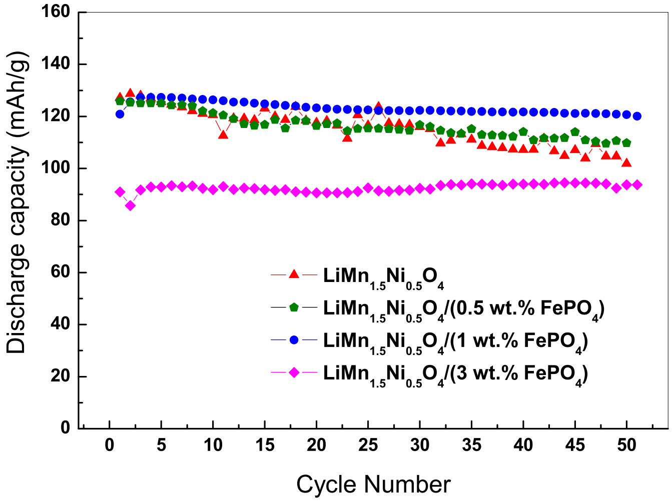

Fig. 4. Cycling performances of the pristine and surface-modified LMNO electrodes.

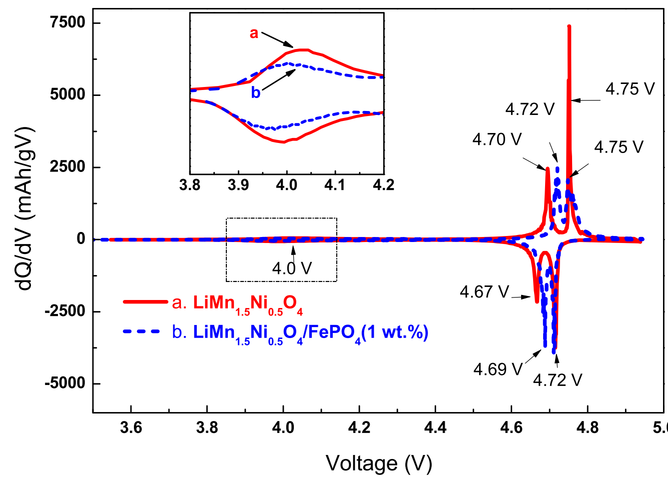

Fig. 6. dQ/dV vs. voltage curves of the pristine (a) and 1 wt.%-coated LMNO (b).

Fig. 5 shows the charge–discharge profiles of the first and 50th cycles at 0.1 C rate. For the pristine and 1 wt.% $FePO_4$-coated electrodes, two plateaus around 4.7 V are clear, consistent with previous reports [7]. The Coulombic efficiencies of the pristine and modified electrodes are 96.2% and 89.9% for the initial cycle, and then increase to 99.3% and 98.9% for the 50th cycle, respectively. The lower initial Coulombic efficiency of the modified LMNO may be due to the insulating coating layer which has not been activated initially. It is interesting to note that the two distinct plateaus at about 4.7 V become indistinguishable with increasing the $FePO_4$ weight ratio and integrated plateaus were exhibited for 3 wt.% $FePO_4$-coated electrode (not shown), which will be directly displayed in dQ/dV curves hereinafter. The plateau around 4.0 V in 1 wt.% $FePO_4$-coated samples becomes increasingly sloped than that of the pristine one, which can be further demonstrated in the inset of Fig. 6.

To clearly observe the redoxes, dQ/dV profiles of the pristine and 1 wt.% $FePO_4$-coated materials in the first cycle are illustrated in Fig. 6. The two dominant peaks around 4.7 V are due to the Ni redox reactions of Ni^{2+}/Ni^{3+} and Ni^{3+}/Ni^{4+} couples, and small redox peaks appear near 4.0 V can be attributed to the redox reaction of Mn^{3+}/Mn^{4+} couples. There is no obvious change in the peak position located at 4.75 and 4.72 V, when comparing the pristine sample to the 1 wt.%-coated one. Nevertheless, the oxidation peak located at 4.70 V shifts to 4.72 V and the reduction peak located at 4.67 V shifts to 4.69 V. The shift of redox potential with an increased trend can be attributed to the disorder–order transition [27], that part of the Fd3m phase converts to $P4_332$ phase for some reason. As can be observed in the inset of Fig. 6, the area of the weak peak around 4.0 V for 1 wt.% $FePO_4$-coated material is obviously lower than that of the pristine one, indicating the capacity decrease in this voltage region after $FePO_4$ coating. This phenomena can be attributed to the increase of the percentage of $P4_332$ phase in the modified electrode, which has higher content of Mn^{4+} and shows cation ordering in the framework, as reported by Hagh et al. [8]. The $Li_xNi_{1-x}O$ phase disappeared in the XRD results possibly derives from that the inside Ni atom transfers to the main spinel LMNO phase where these Ni^{2+} ions will participate in electrochemical reaction. So in this case, such disorder–order transition will increase the original capacity in the modified samples to some extent. On the other side, the essential electrochemical inactive coating material of $FePO_4$ will definitely decrease the initial specific capacity.

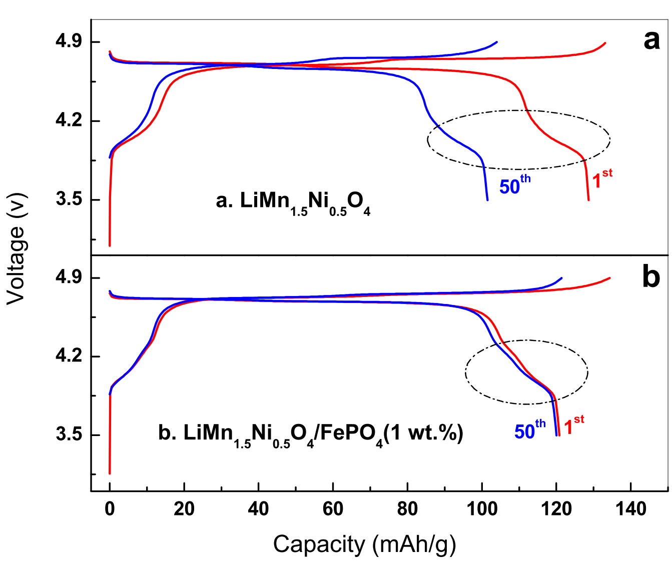

Fig. 5. Galvanostatic curves of the pristine (a) and 1 wt.%-coated LMNO (b).

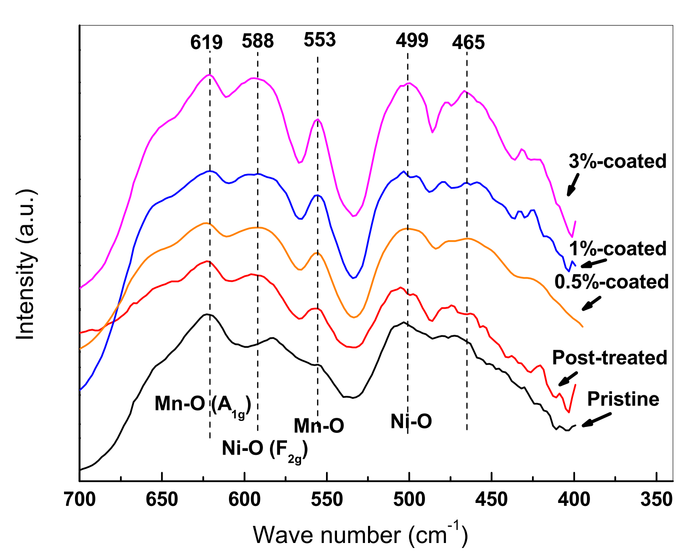

Fig. 7. FTIR spectra of the pristine, post-treated and surface-modified LMNO.

FTIR spectra are measured to ascertain whether $FePO_4$ coating layer plays an important role in disorder–order transition. In Fig. 7, the post-treated material, which has experienced post-annealing at 550 °C for 6 h, is tested and compared with the pristine sample. As shown in Fig. 7, there are distinctive bands in the FTIR spectra, in accordance with the experimental results reported in literature [30]. Generally, the pristine LMNO shows relative softed bands with low intensities. After post-treatment, these bands become sharp and exhibit higher intensities. It has been reported by Kunduraci [30] that though the temperature of post-annealing is less than the onset of order–disorder transition (712 °C), part of the disordered phase of LMNO will transform to ordered phase in the spinel framework. Obviously, the post-treated sample shows a trend of disorder–order transition in contrast with the pristine one. Specifically, the surface-modified samples exhibit more sharp bands with higher intensities than those uncoated ones. On the other hand, the intensity of 588 cm^{-1} Ni–O band is increased compared with the 619 cm^{-1} Mn–O band, and the intensity of 553 cm^{-1} Mn–O band is developing with the increasing content of $FePO_4$ coating. All of these features support the disorder–order transition in certain extent after surface modification.

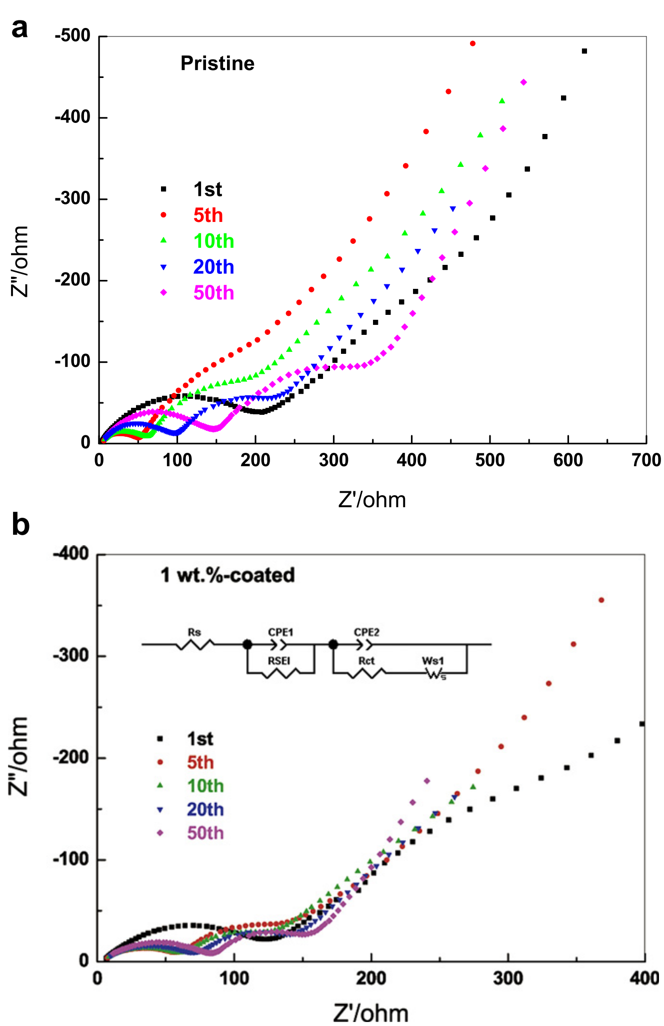

Fig. 8. Nyquist plots of the pristine (a) and 1 wt.%-coated LMNO (b) after different cycles (the unexpectedly large impedance of the first cycle of the electrode arises from fitting error because the semicircles of the first cycle is rather irregular).

Table 2
EIS data of pristine and modified LMNO after different cycles.

Cycle number		1st	5th	10th	20th	50th
R_{sol} (Ω)	Pristine LMNO	2.3	2.9	2.5	2.9	2.7
	1%-coated LMNO	4.2	3.1	2.6	2.1	2.7
R_{SEI} (Ω)	Pristine LMNO	203.7	49.8	61.5	95.9	145.7
	1%-coated LMNO	127.2	61.5	64.3	66.4	84.5

Kunduraci et al. reported that the intensity ratio of two bands at 619 and 588 cm^{-1} can be used to assess percentage of ordered phase in spinel [27].Taken this into account, it can be drawn that the surface-modified samples show a higher percentage of ordered phase than those uncoated ones. This can be attributed to the post-treatment procedure in $FePO_4$ coating process, which is in favor of the disorder–order transition. However, the percentage of ordered phase is very low in all of these samples, for the main phase in this framework is Fd3m, as confirmed by FTIR spectra. To sum up the FTIR results, post-annealing in $FePO_4$ coating process is in favor of the disorder–order transition.

To understand the improved cyclability of surface-modified LMNO, the cells were aged for two days to reach equilibrium before AC impedance data were recorded. The EIS spectra of pristine and 1 wt.% $FePO_4$-coated samples at different cycles were shown in Fig. 8. In Nyquist plot, the first semicircle in high-frequency region can be mainly ascribed to the contribution of solid electrolyte interphase (SEI) film on the electrode (R_{SEI}) [31]. The second semicircle in medium frequency region is assigned to charge transfer reaction (R_{CT}), and the slope in low frequency is attributed to lithium-ion diffusion in bulk material [32]. The equivalent circuit was depicted in the inset of Fig. 8(b), and parameters in Table 2 were determined by plot fitting with it. Clearly, all R_{sol} data are rather low and can be negligible. It is seen that the impedance of the pristine LMNO electrode increases sharply with cycling while that of the 1 wt.% $FePO_4$-coated electrode increases very slowly.

As the pristine and 1 wt.% $FePO_4$-coated LMNO are different electrodes, their impedances cannot be quantitatively compared directly. The R_{SEI} value of each electrode after 5 cycles at discharge state is defined as 1 (normalized) [33]. The evolutions of the impedance of these two materials with cycling are compared in Fig. 9. The impedance of the pristine electrode increases rapidly with cycling while that of 1 wt.% $FePO_4$-coated electrode increases very little. Liu et al. reported that the constant increase of

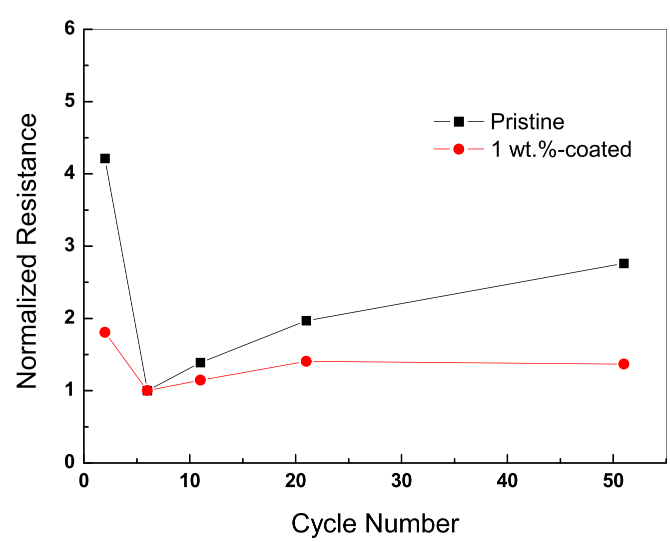

Fig. 9. Comparison of normalized impedance of the cells after different cycles.

impedance in electrode is possibly due to the formation of thicker SEI layer by the severe oxidation of electrolyte at a very high potential [19]. In this case, with the existence of inactive $FePO_4$ layer, which reduces the contact between electrode and electrolyte, however, shows smaller impedance change in repeated cycling. Suppression of the impedance increasement is favorable for elongating the lifetime of a cell, which partly explains the enhanced cyclability of the modified material. Further work is in progress to confirm this suggestion and will be published elsewhere.

4. Conclusions

$FePO_4$-coated LMNO materials with different weight ratios were prepared by chemical deposition. The thickness of 1 wt.% $FePO_4$ coating layer is determined to be 4 nm by TEM observation. Experimental results show that 1 wt.% $FePO_4$-coated LMNO cathode exhibits excellent cycling stability compared with the pristine material. The shift of redox potential confirms a disorder–order phase transition, that a small fraction of the Fd3m phase converts to the $P4_332$ phase. FTIR spectra reveals that $FePO_4$ coating process can be in favor of the disorder–order transition. The EIS study indicates that the improved cycling performance of the surface-modified samples is partly due to the suppression of the development of SEI layer, which will deteriorate the electrochemical performance of active electrode. Surface modification by $FePO_4$ is an effective way to improve the performance of LMNO cathode materials for lithium-ion batteries.

Acknowledgements

This work was supported by the National Natural Science Foundation of China (50902044 and 60976016), the Program for Innovative Research Team in Science and Technology in University of Henan Province (IRTSTHN) (2012IRTSTHN004), the Innovation Scientists and Technicians Troop Construction Projects of Henan Province (124200510004) and the Natural Science Foundation of Henan Province Department of Education (2010B480004).

References

[1] B. Kang, G. Ceder, Nature 458 (2009) 190–193.
[2] K. Amine, H. Tukamoto, H. Yasuda, Y. Fujita, J. Power Sources 68 (1997) 604–608.
[3] R. Alcantara, M. Jaraba, P. Lavela, J. Tirado, P. Biensan, A. de Guibert, C. Jordy, J. Peres, Chem. Mater. 15 (2003) 2376–2382.
[4] J. Kim, Electrochim. Acta 49 (2004) 219–227.
[5] T. Arunkumar, A. Manthiram, Electrochim. Acta 50 (2005) 5568–5572.
[6] H. Wu, J. Tu, Y. Yuan, Y. Li, X. Zhao, G. Cao, Electrochim. Acta 50 (2005) 4104–4108.
[7] M. Kunduraci, G. Amatucci, Electrochim. Acta 53 (2008) 4193–4199.
[8] N.M. Hagh, G.G. Amatucci, J. Power Sources 195 (2010) 5005–5012.
[9] M. Jo, Y.-K. Lee, K.M. Kim, J. Cho, J. Electrochem. Soc. 157 (2010) A841.
[10] Y. Sun, Y. Yang, H. Zhan, H. Shao, Y. Zhou, J. Power Sources 195 (2010) 4322–4326.
[11] J.M. Amarilla, R.M. Rojas, J.M. Rojo, J. Power Sources 196 (2011) 5951–5959.
[12] J. Liu, A. Manthiram, Chem. Mater. 21 (2009) 1695–1707.
[13] G.B. Zhong, Y.Y. Wang, Z.C. Zhang, C.H. Chen, Electrochim. Acta 56 (2011) 6554–6561.
[14] X. Zhang, J. Liu, H. Yu, G. Yang, J. Wang, Z. Yu, H. Xie, R. Wang, Electrochim. Acta 55 (2010) 2414–2417.
[15] H. Wang, T.A. Tan, P. Yang, M.O. Lai, L. Lu, J. Phys. Chem. C 115 (2011) 6102–6110.
[16] M. Aklalouch, J.M. Amarilla, R.M. Rojas, I. Saadoune, J.M. Rojo, Electrochem. Commun. 12 (2010) 548–552.
[17] J. Liu, B. Reeja-Jayan, A. Manthiram, J. Phys. Chem. C 114 (2010) 9528–9533.
[18] R. Singhal, M.S. Tomar, J.G. Burgos, R.S. Katiyar, J. Power Sources 183 (2008) 334–338.
[19] J. Liu, A. Manthiram, J. Electrochem. Soc. 156 (2009) A833.
[20] J.Y. Shi, C.-W. Yi, K. Kim, J. Power Sources 195 (2010) 6860–6866.
[21] T. Yang, N. Zhang, Y. Lang, K. Sun, Electrochim. Acta 56 (2011) 4058–4064.
[22] G. Li, Z. Yang, W. Yang, J. Power Sources 183 (2008) 741–748.
[23] C. Qing, Y. Bai, J. Yang, W. Zhang, Electrochim. Acta 56 (2011) 6612.
[24] H. Lee, Y. Kim, Y.-S. Hong, Y. Kim, M.G. Kim, N.-S. Shin, J. Cho, J. Electrochem. Soc. 153 (2006) A781.
[25] Z. Yang, S. Li, S.A. Xia, Y. Jiang, W.X. Zhang, Y.H. Huang, Electrochem. Solid-State Lett. 14 (2011) A109.
[26] H. Duncan, Y. Abu-Lebdeh, I.J. Davidson, J. Electrochem. Soc. 157 (2010) A528.
[27] M. Kunduraci, G.G. Amatucci, J. Electrochem. Soc. 153 (2006) A1345.
[28] T.F. Yi, Y.R. Zhu, Electrochim. Acta 53 (2008) 3120–3126.
[29] J.B. Goodenough, Y. Kim, Chem. Mater. 22 (2010) 587–603.
[30] M. Kunduraci, J.F. Al-Sharab, G.G. Amatucci, Chem. Mater. 18 (2006) 3585–3592.
[31] S. Zhang, K. Xu, T. Jow, Electrochem. Solid-State Lett. 5 (2002) A259–A262.
[32] J. Liu, A. Manthiram, J. Phys. Chem. C 113 (2009) 15073–15079.
[33] Y. Bai, Y. Yin, N. Liu, B. Guo, H. Shi, J. Liu, Z. Wang, L. Chen, J. Power Sources 174 (2007) 328–334.